Catalysis Science & Technology

Accepted Manuscript

ROYAL SOCIETY OF CHEMISTRY

www.rsc.org/catalysis

Catalysis Science & Technology

ARTICLE

Hydrodeoxygenation of Karanja Oil over Supported Nickel Catalysts: Influence of Support and Nickel Loading

Received 03rd september 2015,
Accepted 00th September 20xx

DOI: 10.1039/x0xx00000x

www.rsc.org/

Sudhakara Reddy Yenumala,[a] Sunil K. Maity[a,*] and Debaprasad Shee[a]

Production of hydrocarbon transportation fuels from triglycerides is extremely important to reduce enslavement on limited fossil fuels. Present article provides a systematic examination of hydrodeoxygenation (HDO) of karanja oil (KO) in a semi-batch reactor over supported (γ-Al_2O_3, SiO_2, and HZSM-5) nickel catalyst. The catalysts were associated with both dispersed and bulk nickel/nickel oxide depending on extent of nickel loading and nature of support. Virgin KO is composed of ~76 wt% C_{18} fatty acids with ~15 wt% oxygen. HDO of KO resulted in a wide range of alkanes (C_{10}-C_{22}) with n-heptadecane being the major one. Transformation of KO into alkanes proceeds through three distinct routes: HDO, catalytic cracking, thermal cracking, or their combination. Highly acidic catalyst (HZSM-5 and Ni/HZSM-5) promotes catalytic cracking leading to formation of large extent of lighter alkanes. Cracking reaction becomes significant over γ-Al_2O_3 supported nickel catalyst with ≤15 wt% nickel loading at elevated temperature. Strong metal-support interaction favored HDO pathway over γ-Al_2O_3 supported nickel catalyst with ≥20 wt% nickel loading. About 80 wt% of KO converted to liquid product with physicochemical properties comparable with light diesel oil.

1 Introduction

Transportation fuels play extremely vital role in the daily life of today's modern civilization. At present, the transportation fuels are predominantly derived from finite fossil fuels. It is the world's single largest energy consuming sector with annual intake of ~27.0 quadrillion Btu alone (total energy consumption is ~97.1 quadrillion Btu).[1] On the other hand, the transportation fuels consumption of the globe is growing continuously with gradual rise of population and standard of living. Continuous depletion of fossil fuels, escalation of transportation fuels price, and deterioration of environmental cleanliness are the primary motives to explore carbon-neutral renewable transportation fuels for sustainability of the biosphere as a whole.

The bio-fuels derived from renewable biomass are the attractive alternatives to substitute fossil fuels based transportation fuels. The bio-fuels offer additional benefits of reduction of carbon footprint and greenhouse gas emissions in the atmosphere as well as improvement of rural economies and national energy security.[2] The annual consumption of the major liquid transportation fuels (gasoline, aviation turbine fuel, and diesel) in India was 8.53×10^{07} metric tons during 2011-2012 with more than 75% share of diesel fuel alone.[3] The biodiesel has thus been attracted huge attention globally as a potential substitute of petro-diesel. The biodiesel is generally produced by transesterification of triglycerides (vegetable oil, animal fat, waste cooking oil, and microalgal oil) with methanol in presence of alkali catalysts. The unfavourable cold flow properties however limit application of biodiesel as blending with petro-diesel to the extent of 20 wt% only for direct use in unmodified internal combustion engine.[4-5] Moreover, the presence of oxygen in biodiesel results in lower calorific value and hence lesser mileage compared to petro-diesel. These factors debarred widespread acceptability of biodiesel globally so far. Therefore, methods of production of hydrocarbon analogous liquid transportation fuels from biomass are highly essential for shifting dependency away from limited fossil fuels.[6-7]

Triglycerides are promising feedstocks for production of hydrocarbon transportation fuels due to their simplicity in chemical structure and lower content of oxygen compared to cellulosic biomass. Moreover, the triglycerides are composed of C_8-C_{24} fatty acids with majority being C_{16} and C_{18}.[8] Therefore, removal of oxygen heteroatoms from triglycerides results in diesel range hydrocarbons commonly known as green diesel.[6-7,9] Several methodologies were thus explored in the past to produce green diesel from triglycerides including pyrolysis[2,10] and catalytic cracking.[11-12] These methodologies are however not adequate to reduce carbon losses of triglycerides leading to low yield of liquid hydrocarbons. On the other hand, the hydrodeoxygenation (HDO) in presence of high hydrogen pressure is a promising approach for the production of green diesel in high yield from triglycerides. HDO

[a] Department of Chemical Engineering, Indian Institute of Technology Hyderabad, Kandi, Sangareddy -502285, Telangana, India. *Corresponding author (Dr. Sunil K. Maity): Phone: +91-40-2301-6075; Fax: +91-40-2301 6003; E-mail: sunil_maity@iith.ac.in

Electronic Supplementary Information (ESI) available: [Reproducibility and reusability, TPD profile, chromatogram of FAME, karanja oil, liquid product and gas sample, effect of atmosphere, FTIR and TGA of spent catalyst]. See DOI: 10.1039/x0xx00000x

involves several consecutive reactions that led to removal of oxygen in the form of water and CO/CO_2. HDO yields high cetane (more than 80) green diesel with low concentration of aromatics and negligible sulfur content.[13]

Several researchers thus studied HDO of pure triglycerides,[14] sunflower oil,[15-21] rapeseed oil,[22-25] waste cooking oil,[26-28] and jatropha oil.[29-32] Alumina, mesoporous silica (SBA-15 and MCM-41), and zeolite (HZSM-5 and HY) supported several metals (Ni, Co, Mo, W, Pt, and Pd) were tested as catalyst. The HDO of sunflower oil over commercial hydrocracking catalyst at 673-693 K and 180 bar H_2 resulted green diesel with properties similar to petro-diesel.[21] During HDO of tripalmitin over Pt/γ-Al_2O_3, pentadecane (PD) was observed as major product with insignificant quantity of hexadecane.[33] For HDO of sunflower oil over Pd/Al-SBA-5, low yield of diesel-like hydrocarbons was observed for catalyst with strong acidity at high temperature.[17] From the above discussion, it is quite clear that systematic examination of HDO of inedible karanja oil (KO) was not attempted until now. India has estimated annual production potential of ~20 million ton inedible oil seeds (e.g. karanja, neem, mahua etc) with only a few percentage of utilization with the share of karanja oil seeds being 0.2 million ton alone.[6] The present work was thus commenced on HDO of KO over supported nickel catalyst in a semi-batch reactor for production of green diesel. The comprehensive investigation was carried out to articulate roles of acidity of the catalysts, nickel loading on γ-Al_2O_3, and temperature on conversion of oxygenates and product distribution. Furthermore, the physicochemical properties of the liquid product were measured to demonstrate its suitability as transportation fuel.

2 Experimental

2.1 Materials

Nickel nitrate hexahydrate (≥97%), and carbon tetrachloride (99.8%) were procured from Merck Specialties Pvt. Limited. γ-Al_2O_3, SiO_2 (AEROSIL-200), and HZSM-5 (SiO_2/Al_2O_3 mole ratio = 80) were obtained from Alfa Aesar, Nippon Aerosil Co. Ltd., and Zeolyst International respectively. KO was procured from Maruti Agro Ltd., India. n-Dodecane (anhydrous, ≥99%) was purchased from Sigma-Aldrich. All chemicals were used without further purification.

2.2 Catalyst preparation and characterization

Supported nickel catalysts, xNiS (x wt% nickel supported on S (Al, Si, and ZSM for γ-Al_2O_3, SiO_2, and HZSM-5 respectively)), were prepared by incipient wetness impregnation method. The catalyst was dried at 373 K for 6 h. The dried material was then calcined at 823 K for 6 h followed by reduction in presence of hydrogen at 823 K for 3 h in a tubular furnace.

The specific surface area was calculated from nitrogen adsorption isotherm using multi point BET equation. The isotherm data was collected at 77 K (Micromeritics ASAP 2020 physisorption analyser) in the relative pressure (P/P0) range of 0.05 to 0.3. The pore volume was considered as the volume of nitrogen adsorbed at P/P^0 of aprox.1. Temperature programmed reduction (TPR), temperature programmed desorption of ammonia (NH_3-TPD), and H_2 pulse chemisorption studies were performed in Micrometrics AutoChem II 2920 chemisorption analyser equipped with a thermal conductivity detector (TCD). Powder X-ray diffraction (XRD) pattern of the catalysts were recorded in the Bragg's angle (2θ) range of 10° to 90° with a scan rate of 1^o/min in a Phillips X-ray diffractometer (X-PERT Pro PAN analytical) consisting of a CuKα source (λ=1.5418Å) using 30 mA current and 45 kV.

2.3 Experimental setup and procedure

Catalytic activity of supported nickel catalysts for HDO of KO was evaluated in a 300 ml stainless steel semi-batch reactor (Parr Instruments) equipped with a four blade impeller. The reactor temperature was maintained by an electrically heated furnace whose temperature was controlled by a PID controller within ±1 K. The reactor was equipped with a gas inlet valve in the upstream which was connected to a hydrogen cylinder through a mass flow controller. Measured quantity of KO and catalyst were first loaded into the reactor and then pressurized to 20 bar H_2. The reactor was subsequently heated to 473 K and kept there for 1 h for complete hydrogenation of unsaturated triglycerides. The reactor temperature was further ramped to desire reaction temperature with concurrent rising of pressure to 35 bar. After reaching desired pressure, continuous flow of hydrogen gas (100 ml/min) was maintained throughout the reaction. The reactor pressure was controlled by a back pressure regulator which was connected to a gas outlet valve through an intermediate condenser and a gas-liquid separator. The liquid samples were collected through sampling port at regular intervals. The liquid samples diluted with CCl_4 were quantified by GC (Shimadzu, GC-2014) equipped with a flame ionization detector (FID). The compounds of liquid sample were identified using GC-MS (Shimadzu GCMS-QP2010 ultra). The gas sample was analysed by GC connected to TCD.

2.4 Characterization of karanja oil and liquid product

Acid value and iodine value were measured by simple acid-base titration and standard iodometric titration (AOAC, 1999) method respectively.[34] The KO was first converted to fatty acid methyl ester (FAME) by transesterification with methanol under reflux condition using H_2SO_4 as catalyst. FAME composition of KO was then measured by a GC armed with FID. The density (at 298 K), viscosity (at 313 K), and elemental composition (CHNS-O) of virgin KO and liquid product were measured by specific gravity bottle, rheometer (Anton-Parr, MCR-302), and elemental analyser (M/s. Thermo Fisher Scientific, Flash 2000) respectively. Lower calorific value of liquid product was measured using bomb calorimeter (Toshniwal Technologies Pvt. Ltd.). The pour point of liquid product was measured using pour point apparatus (IP-15/291, ASTM – D97/2500) (NIVTECH-CLP4). The flash and fire point of liquid product were measured by flash and fire point apparatus (ASTM – D92) (Global Technologies) using open cup - cleveland method.

3 Results and discussion

3.1 Catalyst characterization

The BET surface area and pore volume of calcined and reduced supported nickel catalysts and supports are shown in Table 1. γ-Al_2O_3, SiO_2, and HZSM-5 have surface area of 240, 208, and 402 m^2/g respectively. The surface area and pore volume of supported nickel catalysts were slightly lower than pure supports due to coverage of surface and blockage of pores by nickel oxide/nickel. Furthermore, the surface area and pore volume of γ-Al_2O_3 supported nickel catalysts shrank continually with increasing nickel loading on γ-Al_2O_3. Moreover, reduced γ-Al_2O_3 supported nickel catalysts showed slightly lesser surface area than calcined catalysts. It may be due to sintering and agglomeration of nickel particles during the reduction.

Table 1 BET surface area, H_2 pulse chemisorption results, acidity, and crystallite size of the supported nickel catalysts.

catalysts	surface area, m^2/g		pore volume, cm^3/g		H_2 pulse chemisorption		acidity, mmol/g	crystallite size from powder XRD, nm	
	cal	red	cal	red	MD	S_m	red	cal (NiO)	red (Ni)
γ-Al_2O_3	240		0.83		-	-	trace	-	-
10NiAl	222	192		0.69	1.47	9.77	0.21	-	-
15NiAl	194	182	0.63	0.64	1.16	7.71	0.21	28.4	-
20NiAl	183	168	0.58	0.58	1.06	7.08	0.18	36.2	32.0
25NiAl	171	167	0.53	0.57	1.12	7.5	0.18	39.6	35.6
30NiAl	148	141	0.48	0.52	1.09	7.3	0.14	39.3	38.0
SiO_2	208		-		-	-	-	-	-
25NiSi	141	191	0.85	1.38	0.05	0.32	nil	46.7	78.8
HZSM-5	402		0.28		-	-	0.55	-	-
25NiZSM	252	286	0.19	0.22	0.89	5.95	0.27	68.4	136.9

cal= calcined; red= reduced; MD= metal dispersion, %; S_m=metallic surface area, m^2/g metal.

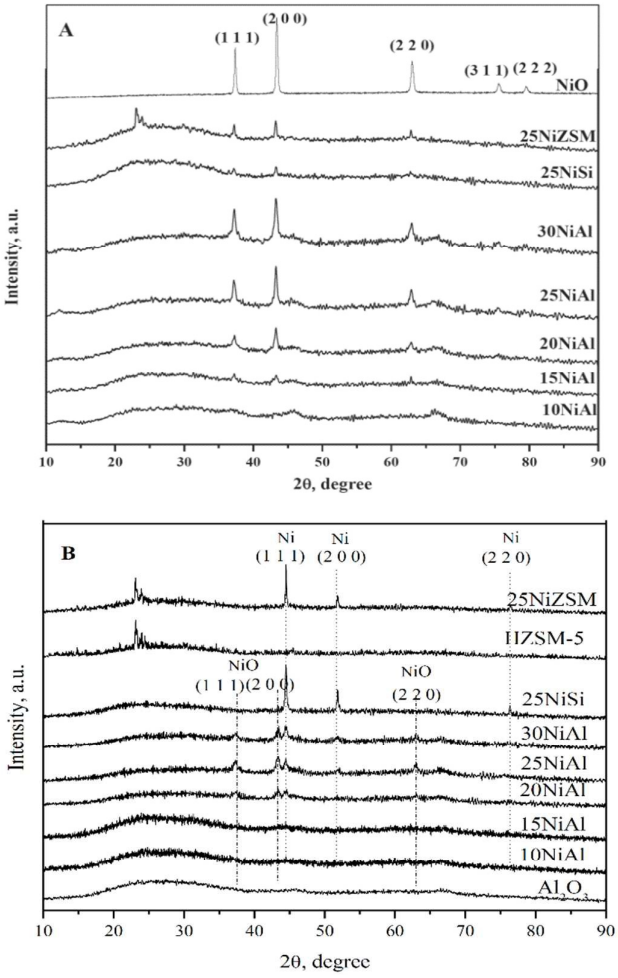

Fig. 1 Powder XRD pattern of (A) calcined and (B) reduced supported nickel catalysts.

The metal dispersion (MD) and metallic surface area (S_m) was virtually similar for γ-Al_2O_3 supported nickel catalysts with ≥15 wt% nickel loading on γ-Al_2O_3 (Table 1). 10NiAl however showed slightly higher MD. On the other hand, 25NiAl showed significantly higher MD and S_m compared to 25NiSi. The possible role of surface area on MD and S_m however can be safely nullified as surface area of γ-Al_2O_3 and SiO_2 are reasonably close. Therefore, from these results it can be indeed concluded that nickel has much stronger interaction with γ-Al_2O_3 than SiO_2 that leads to higher MD and S_m for 25NiAl than 25NiSi. 25NiZSM was however excluded from the comparison of metal-support interaction due to very high surface area of HZSM-5 compared to γ-Al_2O_3 and SiO_2.

Powder XRD pattern of calcined and reduced γ-Al_2O_3, SiO_2, and HZSM supported nickel catalysts together with supports are shown in Fig. 1. Powder XRD pattern of bulk nickel oxide was also included in the figure for clear percipience of various crystalline species in the catalysts. The calcined γ-Al_2O_3 supported nickel catalysts with ≥15 wt% nickel loading on γ-Al_2O_3 exhibited typical diffraction peaks of bulk nickel oxide at 2θ of 37.36° (1 1 1), 43.44° (2 0 0), and 62.88° (2 2 0) (PCPDF# 780643). The 10NiAl however showed only γ-Al_2O_3 diffraction peaks thereby corroborating the presence of well dispersed nickel oxide species. The intensity and sharpness of nickel oxide diffraction peaks increased with increasing nickel loading on γ-Al_2O_3 due to increased amount of well crystalline bulk nickel oxide species. The presence of bulk nickel oxide at elevated nickel loading on γ-Al_2O_3 was also reported earlier.[35-36] Similarly, 25NiSi and 25NiZSM exhibited presence of bulk nickel oxide species.[35]

The reduced supported catalysts with ≥20 wt% nickel loading on γ-Al_2O_3 revealed typical diffraction peaks of bulk nickel at 2θ of 44.4° (1 1 1) and 51.8° (2 0 0) (PCPDF#701849). Reduced γ-Al_2O_3 supported nickel catalysts with ≤15 wt% nickel loading however displayed no diffraction peaks of bulk nickel.

These results clearly suggest that majority of nickel remains in well dispersed form or crystalline size of nickel are too small to be detected by powder XRD. Reduced γ-Al_2O_3 supported nickel catalysts with ≥20 wt% nickel loading on γ-Al_2O_3 showed additional diffraction peaks at 2θ of 37.36° (1 1 1), 43.44° (2 0 0), and 62.88° (2 2 0). The catalysts were reduced (823 K) well above the reduction temperature of bulk nickel oxide (~673 K) as discussed in the subsequent section. Therefore, these diffraction peaks could not be assigned to bulk nickel oxide. These peaks may be due to partial reduction of nickel aluminate ($NiAl_2O_4$) possessing strong interaction with the support.[35] Moreover, intensity of these diffraction peaks increased with increasing nickel loading on γ-Al_2O_3 due to increased extent of $NiAl_2O_4$ species. The average NiO/Ni crystallite size in the calcined/reduced catalysts were calculated from characteristic NiO/Ni peaks in powder XRD pattern using the Scherrer's equation (Table 1). The NiO crystallite size in calcined 10NiAl and Ni crystallite size in reduced 10NiAl and 15NiAl were not calculated due to poor intensity of the peaks. The larger Ni/NiO crystallite size in 25NiSi further suggests weaker Ni-SiO_2 interaction than Ni-γ-Al_2O_3.

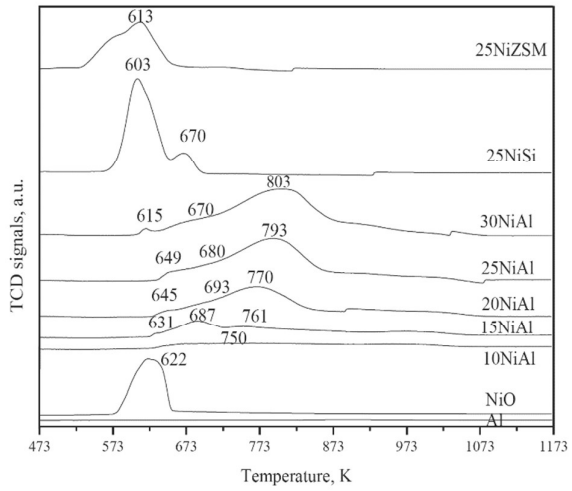

Fig. 2 TPR profile of supported nickel catalysts.

TPR profile together with temperature corresponding to maximum hydrogen consumption (T_{max}) of the calcined catalysts is presented in Fig. 2. The results were further compared with TPR profile of bulk nickel oxide. γ-Al_2O_3 supported nickel catalysts exhibited three distinct reduction peaks in the T_{max} range of 615-649 K, 670-693 K, and 750-803 K. The reduction peak appeared at 615-649 K for γ-Al_2O_3 supported nickel catalysts with ≥15 wt% nickel loading was due to the reduction of bulk nickel oxide with little/no interaction with the support. The reduction peak at T_{max} of 670-693 K was assigned to the reduction of dispersed nickel oxide. The high temperature reduction peak at T_{max} of 750-803 K indicates strong interaction of nickel with γ-Al_2O_3 and was attributed to the dispersed nickel aluminate ($NiAl_2O_4$).[35-36] In general, the Ni^{+2} ions are incorporated in tetrahedral (T_d) or octahedral (O_h) coordinated cation deficient structure of alumina depending on extent of nickel loading.[37] The nickel incorporated in T_d coordinated alumina normally reduces at relatively lower temperature compared to the nickel incorporated in O_h coordinated alumina. The peaks corresponding to the reduction of nickel aluminate shifted gradually to higher temperature with increasing nickel loading on γ-Al_2O_3 due to increased extent of nickel incorporated in O_h coordinated alumina. Powder XRD pattern of reduced catalysts also confirmed nickel aluminate as discussed earlier. The relative magnitude of the reduction peaks further suggests that majority of nickel exists in nickel aluminate form in γ-Al_2O_3 supported nickel catalysts. On the other hand, T_{max} of 25NiSi and 25NiZSM matched closely with the reduction temperature of bulk nickel oxide. These results clearly demonstrate that majority of nickel oxide is present in the bulk form in 25NiSi and 25NiZSM. Moreover, T_{max} signifies extent of metal-support interaction. Higher T_{max} generally indicates stronger metal-support interaction and vice versa. From T_{max} values, it may be further concluded that nickel has much stronger interaction with γ-Al_2O_3 than SiO_2 and HZSM-5.

NH_3-TPD was performed for both supports and reduced supported nickel catalysts as shown in Table 1 (Fig. S1). HZSM-5 is strongly acidic with acidity of 0.55 mmol of NH_3/g; whereas γ-Al_2O_3 is weakly acidic. SiO_2 is however almost neutral. Following impregnation of nickel on HZSM-5, the acidity was somewhat reduced compared to HZSM-5 due to blockage of acidic sites by nickel particles. Reduced γ-Al_2O_3 supported nickel catalyst however exhibited slightly acidic behavior. The acidity of γ-Al_2O_3 supported nickel catalyst might be originated from strong interaction of nickel with γ-Al_2O_3 leading to high MD and T_{max} (Table 1 and Fig. 2). Furthermore, the acidity of reduced γ-Al_2O_3 supported nickel catalyst decreased marginally with increasing nickel loading on γ-Al_2O_3. 30NiAl displayed significantly lower acidity compared to other NiAl catalysts. It may be due to presence of excessive amount of bulk nickel in the catalyst. 25NiSi however remained practically neutral further indicating weak metal-support interaction leading to low MD and T_{max} (Table 1 and Fig. 2).

3.2 Physicochemical properties of karanja oil

The different physicochemical properties of KO are reported in Table 2. The density of KO was 0.97 g/cm^3. The low acid value of 1.23 mg KOH/g signifies presence of negligible amount of free fatty acids in the virgin KO. The iodine value, that represents degree of unsaturation in vegetable oil, was 97.27 g I_2/100 g KO. The viscosity of KO measured at 313 K was 25 cP. The elemental composition showed that native KO is composed of 14.5 wt% oxygen with negligible amount of nitrogen and sulfur. The H/C atomic ratio was 1.76 which was far less than H/C atomic ratio of about 2 for long chain paraffin. FAME composition showed that 76.7 wt% of fatty acids in KO was saturated and unsaturated C_{18} fatty acids (Fig. S2). Only 10.3 wt% fatty acid was palmitic acid (PA) and balance amount being C_{20} and C_{22} fatty acids.

3.3 Reaction mechanism

Analysis of liquid sample collected under different reaction conditions confirmed formation of wide range of linear alkanes

(C_{10} to C_{22}) such as *n*-decane, *n*-undecane, *n*-dodecane, *n*-tetradecane, PD, *n*-hexadecane (HXD), *n*-heptadecane (HPD), *n*-octadecane (OD), *n*-nonadecane, *n*-icosane, *n*-heneicosane, and *n*-docosane with HPD being major one (Fig. S3). In the present work, cumulative amount of lighter alkanes (<PD) and heavier alkanes (>OD) in liquid product was reported throughout the article for simplicity of analysis. Stearic acid (SA), PA, octadecanol (ODL), monostearate (MS), and monopalmitate (MP) were observed as oxygenated intermediates during HDO of KO.

A typical product distribution profile for HDO of KO is shown in Fig. 3. As observed from the figure, wt% of oxygenated intermediates was very high during the initial stage of reaction and decreased gradually with the progress of reaction. On the other hand, wt% of alkanes increased monotonically with increasing reaction time. This result clearly demonstrates that oxygenated intermediates formed during HDO of KO further transform to alkanes during the course of reaction. It may be further observed from the products distribution profile that SA and PA together contributes about 65 wt% of the liquid product at 120 min of reaction. This result clearly suggests that unsaturated triglycerides first undergo saturation in presence of hydrogen over supported metal catalyst. Under high hydrogen pressure, the saturated triglycerides further transformed to fatty acids through intermediate di- and mono-glycerides over supported metal catalysts with release of equivalent amount of propane. The gas phase analysis also confirmed formation of propane as one of the gaseous product. The di-glycerides are however not detected during the reaction. Moreover, concentration of mono-glyceride was negligibly small even at 120 min of reaction. These results clearly suggests that the conversion of triglycerides to fatty acids is relatively fast compared to conversion of fatty acids to alkanes.

Table 2 Physicochemical properties and elemental composition of KO and green diesel, FAME composition of KO, and chemical composition of green diesel.

	KO	Green diesel[a]	FAME composition of KO, wt%[b]	
Density at 298 K, g/cm^3	0.97	0.857	Hexadecanoic (16:0)	10.3
Viscosity at 313 K, cP	25.0	3.81	Octadecanoic (18:0)	7.4
Acid value, mg KOH/g oil	1.23	-	cis-9-Octadecenoic (18:1)	53.5
Iodine value, g I_2/100g oil	97.27	-	cis-9,cis-12- Octadecadienoic (18:2)	15.8
Calorific value, kJ/kg	-	39940	Eicosanoic (20:0)	3.7
Flash point, K	-	411	11 Eicosanoic (20:1)	1.7
Fire point, K	-	418	cis-11,14,17 Eicosatrienoic (20:3)	1.2
Pour point , K	-	282	Docosanoic acid (22:0)	6.4
Elemental composition, wt%			Chemical composition of green diesel, wt%[a]	
C	73.7	85.45	<PD	12.8
H	10.8	14.02	PD	12.9
N	1.0	0	HXD	5.2
S	0	0	HPD	42.3
O	14.5	0.53	OD	4.3
H/C	1.76	1.97	>OD	18.1
Liquid yield, %[c]		80	SA	4.4
Hydrogen consumption, g H_2/g oil [d]		0.05		

Reaction conditions: [a]653 K, 35 bar H_2, 4 (w/w)% 25NiAl, 100 ml H_2/min, 100 g KO, and 600 min. [b] 343 K, 10 g KO, 50 g methanol, 5 ml H_2SO_4, and180 min. [c] 653 K, 35 bar H_2, 4 (w/w)% 25NiAl, 100 ml H_2/min. [d] 613 K, 30 bar H_2, 10 (w/w)% 20NiAl, 5 (w/v)% KO in n-dodecane.

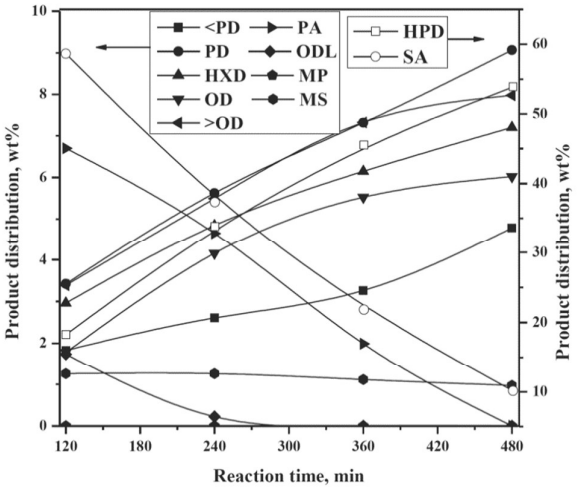

Fig. 3 A typical product distribution profile for HDO of KO. Reaction conditions: 653 K, 35 bar H_2, 4(w/w)% 25NiAl, 100 ml H_2/min.

The fatty acids further transformed to alkanes through different reaction pathways. In order to verify probable conversion of fatty acids to alkane through decarboxylation/decarbonylation route, independent experiments were conducted using SA under nitrogen pressure under otherwise similar experimental conditions.[9] However, conversion of SA was negligible. The possibility of decarboxylation/decarbonylation of fatty acid was thus safely negated by these independent experiments in absence of hydrogen. On the other hand, small quantity of ODL was observed during initial stage of the reaction. It may thus be concluded that fatty acids first reduce to corresponding alcohol in the presence of hydrogen over supported metal catalyst. The alcohols subsequently transform through two different routes forming alkanes with number of carbon atoms either (i) one less than or (ii) equal to corresponding alcohol as shown in Scheme 1. In the first route, the alcohol undergoes dehydrogenation followed by decarbonylation over metallic center of the catalyst forming alkane with one carbon atom less than corresponding alcohol. In the second route, the alcohol undergoes dehydration (over acidic sites of the catalyst) followed by hydrogenation (over metallic sites of the catalyst) forming alkane with same number of carbon atom as

in alcohol. HPD was observed as the major product during HDO of KO under the experimental conditions. On the other hand, KO is composed of 76.7 wt% of C_{18} fatty acids (Table 2). It may therefore be concluded that former route is dominating one for HDO of KO over supported nickel catalyst leading to HPD as primary product.

The KO is also composed of significant amount of C_{16} (10.3 wt%) and C_{20} – C_{22} (13 wt%) fatty acids. Therefore, based on the proposed reaction mechanism, only C_{15} to C_{22} range alkanes are expected as products from HDO of KO. However, substantial amount of C_{10} to C_{14} alkanes were additionally observed as products. This result clearly suggests that oxygenated intermediates or alkanes formed during HDO of KO undergo thermal/catalytic cracking leading to formation of C_{10} to C_{14} alkanes. The lighter alkanes (<PD) were quite significant over highly acidic HZSM-5 and 25NiZSM thereby supporting the above statement.

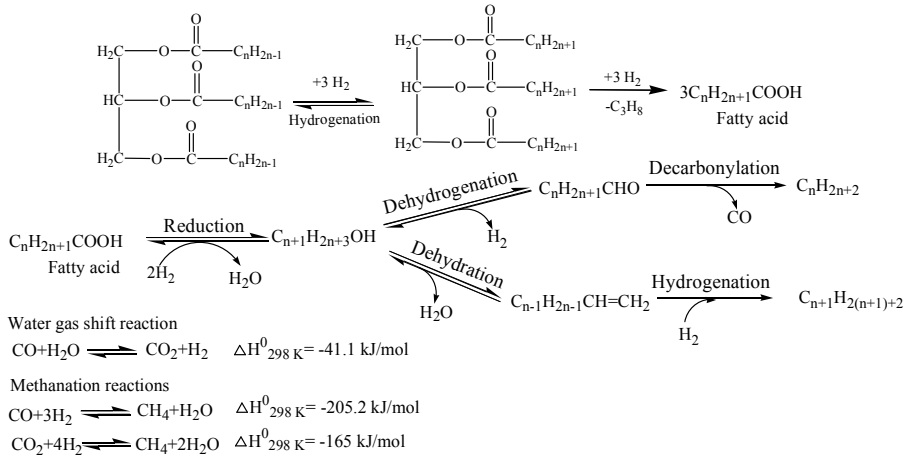

Scheme 1 Possible reaction pathway for HDO of KO over supported nickel catalyst.

Analysis of gas sample confirmed formation of CO, CO_2, CH_4, and C_3H_8 during HDO of KO (Fig. S4). The thermodynamically favorable water gas shift and methanation reaction might be responsible for formation of CO_2 and CH_4 during HDO of KO under the experimental conditions. In order to check possibility of direct conversion of KO to hydrocarbons in absence of hydrogen, an independent experiment was conducted under high nitrogen pressure under otherwise identical experimental conditions (Fig. S5). Significant amount of lighter hydrocarbons were observed as product. This result clearly shows that triglycerides also undergo cracking to form hydrocarbons especially at elevated temperature over acidic catalyst or supported metal catalyst with low metal loading (as discussed in subsequent section).

3.4 Reproducibility and reusability of 20NiAl and external mass transfer resistance

To check repeatability of HDO of KO, two independent experiments were performed under identical experimental conditions as shown in Table S1. The conversion of oxygenates and product distribution was practically similar for both the runs thereby confirming the reproducibility of the experiments. The spent catalyst of the two independent repeatability experiments was filtered from the reaction mixture, washed repeatedly with ethanol (to remove adsorbed organics), and then dried at 373 K for 24 h. A fresh experiment on HDO of KO was then conducted using the spent catalyst under similar experimental conditions. The spent catalyst showed significantly lower catalytic activity compared to fresh catalyst. The reduced catalytic activity of spent catalyst may be due to presence of adsorbed hydrocarbons and oxygenates and formation of coke as observed from FTIR and TGA results (Fig. S6 and S7). We further extended the work to regenerate the spent catalyst by calcination followed by reduction at 823 K. The conversion of oxygenates and product distribution over regenerated catalyst was essentially comparable with the fresh catalyst thereby demonstrating regeneration ability of the catalyst. HDO of KO was also performed at several speed of agitation to negate existence of external mass transfer resistance in the reaction. The conversion of oxygenates and product distribution remained practically unaffected beyond 1000 rpm demonstrating absence of external mass transfer resistance in the reaction.

3.5 Role of supports

HDO of KO was investigated over various supported (γ-Al_2O_3, SiO_2, and HZSM-5) nickel catalyst with identical nickel loading (25 wt%) to apprehend role of acidity on conversion of oxygenates and product distribution. HZSM-5 supported nickel catalyst showed slightly higher catalytic activity compared to γ-Al_2O_3 and SiO_2 supported nickel catalyst as shown in Fig. 4. 25NiZSM showed 94% conversion of oxygenates at 480 min of reaction compared to only 89% and 75% conversion of oxygenates for 25NiAl and 25NiSi respectively. The superior catalytic activity of 25NiZSM might be due to its higher surface area and stronger acidity than 25NiAl and 25NiSi (Table 1). The HPD was observed as the major liquid product for all the catalysts. About 55 wt%, 45 wt%, and 33 wt% of the alkanes in liquid product was HPD for 25NiAl, 25NiSi, and 25NiZSM respectively. On the other hand, wt% of lighter alkanes (<PD) was maximum for 25NiZSM followed by 25NiSi and 25NiAl. The catalytic cracking of oxygenated intermediates or alkanes favors over highly acidic 25NiZSM catalyst leading to higher wt% of lighter alkanes in liquid product. Duan et al. also

reported similar observation for HDO of sunflower oil.[17] The lower tendency of catalytic cracking over 25NiAl might be due to strong metal-support interaction as reflected by high MD and S_m (Table 1) which in turn favors HDO reaction.

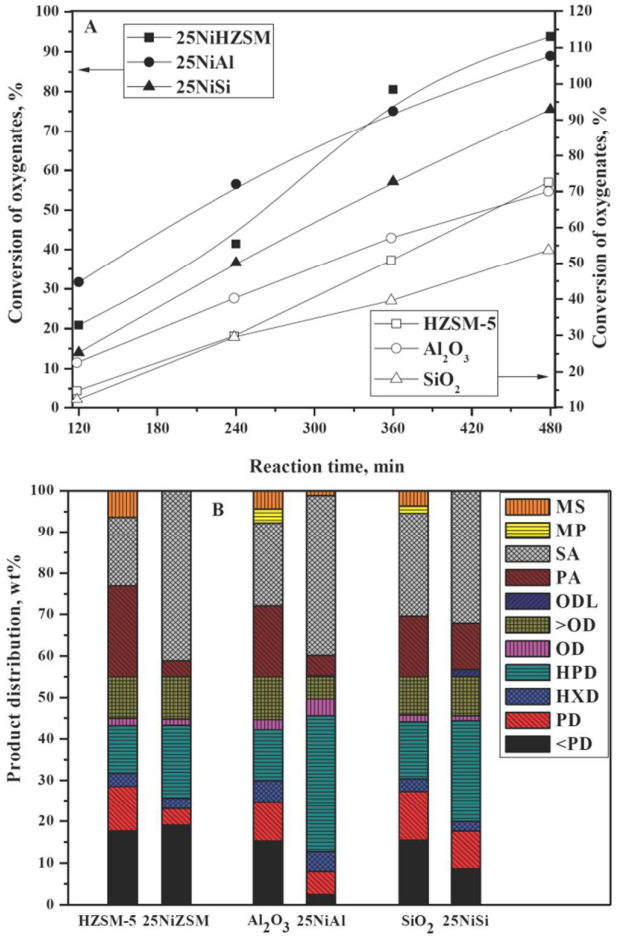

Fig. 4 Effect of support on (A) conversion of oxygenates and (B) product distribution at 55% conversion of oxygenates. Reaction conditions: 653 K, 35 bar H_2, 4 (w/w)% catalyst, 100 ml H_2/min.

The study was further extended to pure supports under similar experimental conditions to understand role of supports on HDO of KO as shown in Fig. 4. The trend of conversion of oxygenates was observed in the order of HZSM-5≥γ-Al_2O_3>SiO_2. At 55% conversion of oxygenates, only about 20 wt% of the alkanes in liquid product was HPD for pure supports. The lighter alkanes (<PD) were also slightly higher over HZSM-5 compared to γ-Al_2O_3 and SiO_2. From these results it may be concluded that catalytic cracking of triglycerides was favored over highly acidic support. It may be further observed that supported nickel catalyst showed enhanced catalytic activity compared to respective pure support. Moreover, wt% of lighter alkanes (<PD) was relatively higher for pure support than corresponding supported nickel catalyst. From these results, it may be concluded that nickel promotes HDO of triglycerides thereby reducing formation of lighter alkanes. Since γ-Al_2O_3 supported nickel catalyst demonstrated superior HDO activity with least tendency of catalytic cracking; all subsequent studies were performed using γ-Al_2O_3 supported nickel catalyst.

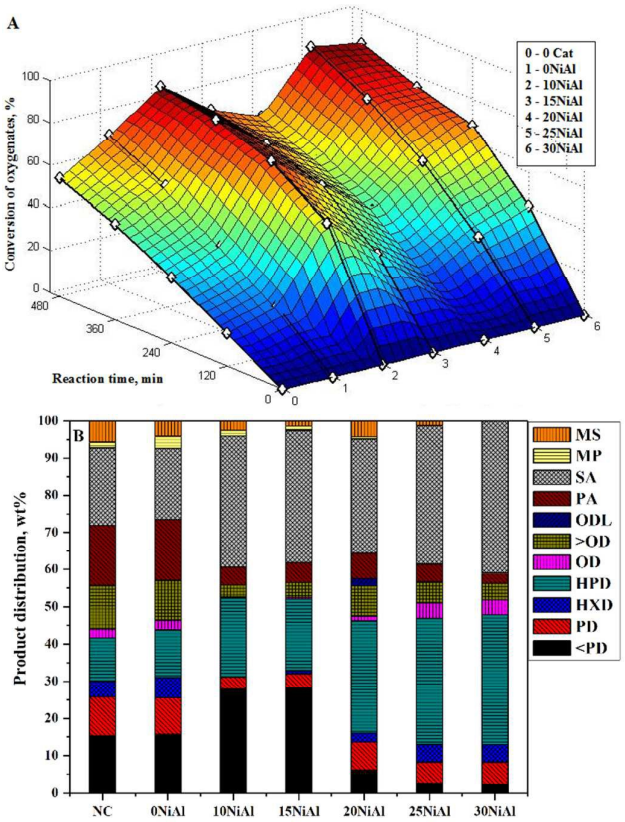

Fig. 5 Effect of nickel loading on (A) conversion of oxygenates and (B) product distribution at 55% conversion of oxygenates. Reaction conditions: 653 K, 35 bar H_2, 4 (w/w) % catalyst, 100 ml H_2/min.

3.6 Effect of nickel loading on γ-Al_2O_3

Diverting the reaction away from thermal/catalytic cracking towards HDO route is highly desirable to improve the yield of liquid product preserving hydrocarbon backbone of the triglycerides. In the present work, HDO of KO was thus investigated over several γ-Al_2O_3 supported nickel catalysts of varying nickel loading (0-30 wt%) to determine optimum nickel loading on γ-Al_2O_3 to minimize cracking reactions. An independent experiment was also conducted without catalyst to quantify extent of thermal cracking under the experimental conditions (Fig. 5). The conversion of oxygenates in absence of any catalyst was about 55% at 480 min of reaction. However, about 68% conversion of oxygenates was observed over γ-Al_2O_3 at 480 min of reaction. The conversion of oxygenates over γ-Al_2O_3 and in absence of any catalyst was mainly due to catalytic/thermal cracking of triglycerides under the experimental conditions. The high wt% of <PD and PD together with low wt% of HPD in the liquid product further supports the above statement. It may be further noted that conversion of oxygenates and product distribution were identical over SiO_2 and without catalyst (Fig. 4 and Fig. 5). It may therefore be concluded that SiO_2 alone is not imparting any role on HDO of

KO. On the other hand, the conversion of oxygenates was somewhat more over γ-Al_2O_3 compared to without catalyst with insignificant variation in product distribution. It clearly indicates that γ-Al_2O_3 promotes catalytic cracking to some extent due to its mild acidity.

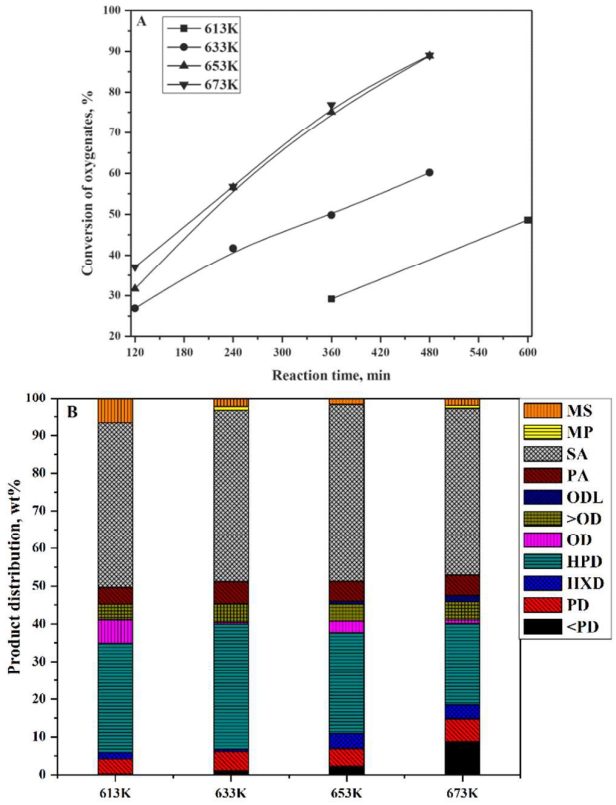

Fig. 6 Effect of temperature on (A) conversion of oxygenates and (B) product distribution at 45% conversion of oxygenates. Reaction conditions: 35 bar H_2, 4 (w/w)% 25NiAl, 100 ml H_2/min.

The conversion of oxygenates was about 87% over 10NiAl at 480 min of reaction. The conversion of oxygenates however decreased gradually with increasing nickel loading on γ-Al_2O_3 (up to 20 wt%). Beyond 20 wt% nickel loading on γ-Al_2O_3, the conversion of oxygenates increased with further increase of nickel loading on γ-Al_2O_3. The product distribution further showed that wt% of major deoxygenated products, HPD and HXD increased continually with increasing nickel loading on γ-Al_2O_3 (up to 25 wt%) with concurrent decline of wt% of lighter alkanes (<PD). Beyond 25 wt% nickel loading on γ-Al_2O_3, the product distribution practically remained unchanged. ODL, MS, and MP were however not observed over 30NiAl. It may be due to slightly higher HDO activity of 30NiAl leading to faster conversion of the intermediates to corresponding alkanes.

The conversion of oxygenates to hydrocarbons mainly proceeds through two parallel pathways: thermal/catalytic cracking and HDO. At relatively lower nickel loading on γ-Al_2O_3, the reaction mainly proceeds through thermal/catalytic cracking route leading to very high conversion of oxygenates with high wt% of lighter alkanes. With increasing nickel loading on γ-Al_2O_3 up to 20 wt%, the number of active metal sites increased (Table 1) that favored HDO route over thermal/catalytic cracking leading to decline of conversion of oxygenates with simultaneous decrease of wt% of lighter alkanes. At sufficiently high nickel loading on γ-Al_2O_3 (25 wt% or more); the cracking suppresses effectively and reaction mainly proceeds through HDO pathway leading to slightly increasing trend of conversion of oxygenates with further increase of nickel loading on γ-Al_2O_3. For increasing nickel loading on γ-Al_2O_3 from 25% to 30%, the conversion of oxygenates however not increased much. It might be due to the presence of excessive amount of HDO inactive bulk nickel oxide in 30NiAl as well its lower surface area, MD, and S_m (Fig. 2). Harnos et al. also reported increasing trends of sunflower oil conversion and yield of diesel range product with increasing nickel loading.[18] It was reported that fatty acid intermediates were not readily converted to alkanes at lower nickel loading and caused deactivation of catalyst. The higher nickel loading facilitated conversion of fatty acids to alkanes through HDO. 25 wt% was thus considered as optimum nickel loading on γ-Al_2O_3 for HDO of KO. All subsequent studies were therefore performed over 25NiAl.

3.7 Effect of temperature

HDO of KO was examined in the temperature range of 613 to 673 K as shown in Fig. 6. The conversion of oxygenates increased with rise of temperature up to 653 K; beyond which conversion of oxygenates remained practically unchanged. The conversion of oxygenates was about 95% at 653 K and 480 min of reaction. On the other hand, wt% of HPD in liquid product decreased gradually with increasing reaction temperature with simultaneous rise of wt% of lighter alkanes (<PD). From this result it may be concluded that tendency of thermal cracking of oxygenated intermediates or alkanes enhanced with rise of temperature leading to formation of large extent of lighter alkanes at elevated temperature. In order to verify extent of thermal cracking, independent experiments were also performed without catalyst under otherwise identical experimental conditions. The conversion of oxygenates was negligibly small below 613 K. However, the conversion of oxygenates was about 55% at 653 K and 480 min of reaction with significant fraction of liquid product being lighter alkanes (<PD) (Fig. 5). The conversion of triglycerides was also reported to be increased with increasing temperature and reached 100% at 633-653 K.[38]

3.8 Physicochemical properties of liquid product

The physicochemical properties of crude liquid product obtained from HDO of KO under optimal experimental conditions were measured to demonstrate its suitability as transportation fuel. The density (0.857 g/cm^3) and viscosity (3.81cP at 313 K) of liquid product was slightly lower compared to pure KO (Table 2). The density, viscosity, and pour point of liquid product was however matched well with the specification of light diesel oil.[39] In general, diesel and jet fuel are composed of C_9–C_{23} (average C_{16}) and C_8–C_{16} hydrocarbons respectively.[40] Chemical composition further showed that liquid product (composed of ~42 wt% HPD, ~31% ≤HXD, and

~22% ≥OD) was chemically analogous to diesel fuel. The elemental composition of liquid product showed H/C atomic ratio of 1.97 thereby demonstrating the characteristics of long chain paraffin (H/C atomic ratio of 2). The flash point (411 K) of liquid product was however slightly higher than light diesel oil due to presence of excessive amount of lighter alkanes as observed from chemical composition. The consumption of huge amount of expensive hydrogen is one of the major challenges of HDO technology. To measure amount of hydrogen consumed during HDO of KO, an independent experiment was performed in a high pressure batch reactor using n-dodecane as solvent till complete conversion of oxygenates. The hydrogen consumption was about 0.05 g H_2/g KO. It was further observed that ~80 wt% of KO was converted to liquid product. Kalnes et al. also reported 75-85 wt% of liquid yield.[41]

4 Conclusions

HDO of KO was investigated in a semi-batch reactor over supported (γ-Al_2O_3, HZSM-5, and SiO_2) nickel catalyst at 35 bar H_2 in the wide range of temperature (613-673 K) and nickel loading (0-30 wt%) on γ-Al_2O_3. Nickel exhibited stronger interaction with γ-Al_2O_3 than SiO_2 and HZSM-5. γ-Al_2O_3 supported nickel catalyst thus demonstrated superior HDO activity with least tendency towards cracking. On the other hand, catalytic cracking become significant over strongly acidic HZSM-5 and 25NiZSM leading to formation of larger extent of lighter alkanes. γ-Al_2O_3 supported nickel catalyst with low nickel loading (≤20 wt%) led to large extent of cracking with high wt% of lighter alkanes. With ≥25 wt% nickel loading on γ-Al_2O_3, the reaction however proceeded largely through HDO pathway. The thermal cracking became prominent above 653 K. The optimal process conditions for maximizing HDO pathway were 653 K and 25 wt% nickel loading on γ-Al_2O_3 at 35 bar H_2. ~80 wt% of KO converted to liquid product with 65 wt% C_{15}-C_{18} hydrocarbons and H/C atomic ratio of 1.97. Physicochemical properties of liquid product were matched reasonably well with the specification of light diesel oil.

5 Acknowledgement

The authors gratefully acknowledge the financial support from Department of Science and Technology, New Delhi, India (DST/TSG/AF/2010/65-G dated 17.11.2011).

6 References

1 http://www.eia.gov/forecasts/aeo/pdf/0383(2015).pdf.
2 J. Xu, J. Jiang, Y. Sun and J. Chen, *Bioresour Technol*, 2010, **101**, 9803.
3 http://petroleum.nic.in/petstat.pdf.
4 W.C. Wang, N. Thapaliya, A. Campos et al., *Fuel*, 2012, **95**, 622.
5 http://www.afdc.energy.gov/fuels/biodiesel_blends.html
6 S.K. Maity, *Renew Sustain Energy Rev*, 2015, **43**, 1427.
7 S.K. Maity, *Renew Sustain Energy Rev*, 2015, **43**, 1446.
8 S.R. Yenumala and S.K. Maity, *Int J Hydrogen Energy*, 2011, **36**, 11666.
9 P. Kumar, S.R. Yenumala, S.K. Maity and D. Shee, Appl Catal A Gen 2014, **471**, 28.
10 A.C.R. Melo, A.S. Araujo and E.F.B. Silva et al., *Fuel Process Technol*, 2011, **92**, 1340.
11 N. Taufiqurrahmi and S. Bhatia, *Energy Environ Sci* 2011, **4**, 1087.
12 E. Buzetzki, K. Sidorová and Z. Cvengrošová et al., *Fuel Process Technol*, 2011, **92**, 1623.
13 A.V. Lavrenov, E.N. Bogdanets, Y.A. Chumachenko and V.A. Likholobov, *Catal Ind*, 2011, **3**, 250.
14 L. Boda, G. Onyestyák and H. Solt et al., *Appl Catal A Gen*, 2010, **374**, 158.
15 S. Kovács, T. Kasza and A. Thernesz et al., *Chem Eng J*, 2011, **176-177**, 237.
16 M. Krár, S. Kovács, D. Kalló and J. Hancsók, *Bioresour Technol*, 2010, **101**, 9287.
17 J. Duan, J. Han and H. Sun et al., *Catal Commun*, 2012, **17**, 76.
18 S. Harnos, G. Onyestyák and D. Kalló, *React Kinet Mech Catal*, 2012, **106**, 99.
19 T.M. Sankaranarayanan, M. Banu, A. Pandurangan and S. Sivasanker, *Bioresour Technol*, 2011, **102**, 10717.
20 O.V. Kikhtyanin, A.E. Rubanov, A.B. Ayupov and G.V. Echevsky, *Fuel*, 2010, **89**, 3085.
21 P. Šimáček, D. Kubička and I. Kubičková et al., *Fuel*, 2011, **90**, 2473.
22 D. Kubička, P. Šimáček and N. Žilkova, *Top Catal*, 2009, **52**, 161.
23 P. Šimáček, D. Kubička, G. Šebor and M. Pospíšil, *Fuel*, 2010, **89**, 611.
24 R. Sotelo-boy, Y. Liu and T. Minowa, *Ind Eng Chem Res*, 2011, **50**, 2791.
25 P. Priecel, L. Čapek and D. Kubička et al., *Catal Today*, 2011, **176**, 409.
26 S. Bezergianni, A. Dimitriadis, T. Sfetsas and A. Kalogianni, *Bioresour Technol*, 2010, **101**, 7658.
27 S. Bezergianni, A. Dimitriadis, A. Kalogianni and P.A. Pilavachi, *Bioresour Technol*, 2010, **101**, 6651.
28 S. Bezergianni, S. Voutetakis and A. Kalogianni, *Ind Eng Chem Res*, 2009, **48**, 8402.
29 S. Gong, A. Shinozaki, M. Shi and E.W. Qian, *Energy Fuels*, 2012, **26**, 2394.
30 Y. Liu, R. Sotelo-Boyás and K. Murata et al., *Energy Fuels*, 2011, **25**, 4675.
31 K. Murata, Y. Liu, M. Inaba and I. Takahara, *Energy Fuels*, 2010, **24**, 2404.
32 R. Kumar, B.S. Rana and R. Tiwari et al., *Green Chem*, 2010, **12**, 2232.
33 A.T. Madsen, E.H. Ahmed and C.H. Christensen et al., *Fuel*, 2011, **90**, 3433.
34 G.H. Jeffery, J. Bassett, J. Mendham, R.C. Denney, 1989, 5th ed. Longman Sci Tech Essex, UK.
35 V.C.S. Palla, D. Shee and S.K. Maity, *RSC Adv*, 2014, **4**, 41612.
36 V. Dhanala, S.K. Maity and D. Shee, *RSC Adv*, 2013, **3**, 24521.
37 P. Priecel, D. Kubička and L. Čapek et al., *Appl Catal A Gen*, 2011, **397**, 127–137.
38 R.K. Sharma, M. Anand and B.S. Rana et al., *Catal Today*, 2012, **198**, 314.
39 https://www.iocl.com/products/LightDieseloil.aspx
40 S.K. Lee, H. Chou and T.S. Ham et al., *Curr Opin Biotechnol,* 2008, **19**, 556.
41 T.N. Kalnes, T. Marker, D.R. Shonnard and K.P. Koers, *Biofuels Technol*, 2008, **7–11**.

GRAPGICAL ABSTRACT

Conversion of oxygenates increased in the order of 25NiSi<25NiAl≤25NiZSM. Catalytic cracking was significant over HZSM-5 and 25NiZSM. HDO route was dominating over Ni/γ-Al_2O_3 with ≥20 wt% nickel loading. Optimal condition for HDO route was 653 K and 25NiAl at 35 bar H_2. Properties of green diesel was comparable with light diesel oil.